UNIVERSITY OF CALIFORNIA
RIVERSIDE

Multi-sensor Wireless System for Fault Detection in Induction Motors

A Thesis submitted in partial satisfaction
of the requirements for the degree of

Master of Science

in

Electrical Engineering

by

Ehsan Tarkesh Esfahani

June 2012

Thesis Committee:

Professor Sundararajan Venkatadriagaram, Co-Chairperson
Professor Bir Bhanu, Co-Chairperson
Professor Ertem Tuncel

The Thesis of Ehsan Tarkesh Esfahani is approved:

Committee Co-Chairperson

Committee Co-Chairperson

University of California, Riverside

Acknowledgments

I thank my committee, without whose help, I would not have been here. I would like to express my most sincere gratitude to Dr. Sundararajan Venkatadriagaram, advisor of this work, for his technical guidance. I am also grateful to Dr. Bir Bhanu, the co-chair of this thesis for his help and suggestion in machine learning.

I would also like to thank my current lab-mates, Shaocheng Wang and Izimi Tan, for their help in data collection, and the former members of our lab, Dr. Xin Xue and Mr.Miaogeng Zhang for their helpful suggestions in nesC programming.

Finally, I like to acknowledge California Energy Commission and American Public Power Association for supporting this work through EISG grant (56544A/09-20) and DEED scholarship respectively.

ABSTRACT OF THE THESIS

Multi-sensor Wireless System for Fault Detection in Induction Motors

by

Ehsan Tarkesh Esfahani

Master of Science, Graduate Program in Electrical Engineering
University of California, Riverside, June 2012
Professor Sundararajan Venkatadriagaram, Co-Chairperson
Professor Bir Bhanu, Co-Chairperson

This research presents a stand-alone multi-sensor wireless system for continuous real-time performance and condition monitoring of induction motors. The proposed wireless system provides a low-cost alternative to expensive condition monitoring technology available through dedicated current signature analysis or vibration monitoring equipment. The system employs multiple sensors (acoustic, vibration and current) mounted on a common wireless platform. The faults of interest are static and dynamic air-gap eccentricity and bearing damage.

The Hilbert-Huang Transform (HHT) of vibration data and power spectral density (PSD) of current and acoustic signals are used as the features in a hierarchical classifier. The proposed wireless system can distinguish a faulty motor from a healthy motor with a probability of 99.9% of correct detection and less than 0.1% likelihood of false alarm. It can also discriminate between different fault categories and severity with an average accuracy of 95%.

Contents

List of Figures

List of Tables

Nomenclature

$\alpha_i(t)$	Instantaneous amplitude in Hilbert-Huang Transform.
β	Bearing contact angle.
ν	Stator time harmonic (1, 3, 5).
$\omega_i(t)$	Instantaneous frequency in Hilbert-Huang Transform.
$\theta_i(t)$	Instantaneous phase in Hilbert-Huang Transform.
D	Pitch diameter of bearing.
d	Ball diameter of bearing.
f_c	Characteristic vibration frequency (f_{vi}, f_{vo} or f_{vb}).
f_r	Rotational Frequency.
f_s	Supplied Frequency.
$f_{current}$	Frequency component of damaged bearing in current.
f_{HE}	High frequency component of eccentricity in current.
f_{LE}	Low frequency component of eccentricity current.

f_{vb} Ball defected bearing harmonics in vibration.

f_{VE} Eccentricity related frequencies in vibration harmonics.

f_{vi} Inner-race defected bearing harmonics in vibration.

f_{vo} Outer-race defected bearing harmonics in vibration.

$h(\omega)$ Hilbert marginal Spectrum.

$H(\omega, t)$ Hilbert Spectrum.

$H[.]$ Hilbert Transform.

k Any Integer.

n Number of bearings ball.

n_d Eccentricity order.

p Number of pole pairs.

R Number of rotor bars.

s Slip.

$u_i(t)$ the ith IMF

Chapter 1

Introduction

This chapter presents the motivation and objective of this thesis. An outline of this dissertation is presented in the second section.

1.1 Motivation and Objective

Reducing the operating cost and saving energy is a critical point to address in Today's manufacturing industries. Across many industries, maintenance activities typically holds 15-40% of manufacturing costs[1]. In the current competitive marketplace, proper maintenance management plays an increasingly important role in maintaining competitiveness. Tavner et al [2] states that only 10 percent of components replaced during a fixed-interval maintenance outages actually need to be replaced at that time. This clearly shows that an effective maintenance management can reduce equipment downtime and minimize waste.

Predictive maintenance is an alternative to fixed-interval maintenance which stops the machine only before there is evidence of impending failure. The key to a

successful predictive maintenance is a robust condition monitoring system that can capture the initiation and growth of an error in the manufacturing equipment[3]. Although the return on investment depends on the specific industry and the equipment involved, Rao [4] states that an investment in monitoring of between $10,000 and $20,000 dollars results in savings of 500,000 dollars a year.

Recently, U.S. Department of Energy (DOE) has identified wireless sensor networks as one of the featured technologies to improve the overall energy efficiency of U.S. industry. This is the main motivation of this research to develop low-cost wireless sensor for efficient health monitoring of industrial motors and other manufacturing equipment. The objective of this thesis is to determine the feasibility of a stand-alone multi-sensor wireless system for continuous real-time performance and condition monitoring of induction motors. The proposed system employs multiple sensors mounted on a common wireless platform with the capability of installation inside the motor on the stator end-coils or outside on the test bed.

The system follows a sensor fusion approach to detect single faults or combinations of faults in their incipient stages and provides early warning of impending problems. The wireless system provides a low-cost alternative to expensive condition monitoring technology available through dedicated current signature analysis or vibration monitoring equipment. The key performance objectives for the wireless system are :

- Detect faults in induction motors with a probability of 99.9% (i.e. probability of missing a fault is less than 0.1%).
- Produce false alarms no more than 5%.

- Have a high accuracy ($> 99\%$) of correctly identifying the nature and severity of the fault. The faults of interest are static and dynamic air-gap eccentricity and bearing damage (inner-outer race damage, damage on cage or lack of lubricant).

1.2 Impact of the Research

The Industrial Productivity Manual [5] estimates energy efficiency increases of about 2% (and as high as 10-15%) can be achieved with preventive maintenance through condition monitoring strategies. The same study found that industrial electrical motor systems in the U.S. consumed about 25% in 1994 [5]. California consumed nearly 280 billion kWh in 2007 [6]. Assuming that the 25% estimate of 1994 [5] is valid for California in 2007, it can be concluded that industrial motors in California consume about 70 billion kWh. 95% of this energy (i.e. 66 billion kWh) is consumed by motors with ratings over 6 hp [5] the most likely candidates for the wireless system. A savings of 2% of this amount would reduce the energy demand of motors by 1.3 billion kWh per year. Assuming the current rate of electricity at 10 cents/kWh, this implies a saving of $130 million per year in energy consumption to the state industry. At a same time, preventive maintenance of motors helps the end-user in 1) Reducing electricity costs 2) Reduced repair costs 3) Reduced production losses from sudden failures. it should be noted that a typical industry such as a paper mill or a process industry or a machining service employs hundreds of motors.

1.3 Outline of Dissertation

This dissertation is organized as follows: Chapter 2 provides a brief background to condition monitoring and faults in induction motors. The emphasis of this chapter are on bearing and air-gap fault detections.

Materials, methods and experimental studies are then described in Chapter 3. The first section of this chapter describes a low-cost wireless sensor network designed for motor health monitoring and fault classification. The wireless sensor nodes with an accelerometer sensor, a microphone, and a hall-effect sensor are developed and implemented in the wireless health monitoring system for induction motors. It also includes the experimental design for testing different motor faults in the test bed.

The second and third section of this chapter (3.2-3.3) covers the data analysis part including feature generation/selection. Hilbert-Hunag transform as the main step in feature selection and is described in detail. The final section of this chapter focus on the classification method used in this study.

The experimental results are presented and discussed in Chapter 4. The validation results demonstrate the effectiveness and generalizability of the wireless system for motor health monitoring and fault classification.

Finally chapter 5 presents conclusions and possible future directions in developing wireless condition monitoring systems for inductive motors.

Chapter 2

Faults in Motors

Induction motors are widely used in a variety of industrial applications and consume a significant portion of energy [5]. Environmental stress and load conditions applied to these motors can cause a malfunction or reduce the efficiency of the motors leading to repair expenses and financial loss due to unexpected downtime. Therefore, to increase the productivity of the plant and to reduce maintenance costs of these systems, reliable condition monitoring and diagnosis is often desired.

The primary problems in induction motors are 1) Air-gap eccentricity 2) Rotor bar damage 3) Bearing damage 4) Stator winding imbalance [2]. These problems are often neither sudden nor independent. Therefore, by using the progressive nature of these problems, a continuous monitoring system can track the faults as they develop and help identify the root cause of faults and prevent the consequent failures.

There has been substantial amount of research into detection of these faults. Most work focuses on motor current signature analysis because the method is non-invasive, convenient and can yield information on a variety of faults [7]. In addition, vibrations [8] and acoustic emissions [9, 10] have also been used for condition monitoring.

Classical spectral analysis (such as instantaneous power FFT) of stator current is commonly used to detect single or combination of multiple faults in steady state conditions [11]. Additionally, to consider the non-stationary behavior and transient effects in induction motors, a variety of time-frequency analysis such as wavelet transforms [12–16], Hilbert-Huang transform [16–18] in combination with different blind source separation methods such as empirical mode decomposition [18, 19], independent component analysis [20, 21] are used. A complete review of invasive and non-invasive detection methods of faults in stator, rotor, bearings and those related to eccentricity can be found in [22] and [23].

In addition, various machine learning and statistical methods such as support vector machine [21, 24], neural networks [25], genetic algorithms [26] and fuzzy logic are developed to increase the accuracy of fault detection.

The state of the art in condition monitoring of induction motor uses wired sensors, usually of a single modality, to track faults which is mostly done offline. The installation and maintenance of these sensors usually increase the motor downtime and cost more than the cost of the sensors themselves.

Wireless sensors are becoming a more feasible monitoring option because they are small and lightweight, and hence can be placed in limited spaces. They can

be mounted on moving parts, thus eliminating the need for flexible connectors, slip rings etc. The sensors require very little power and are inexpensive to install compared to wired sensors.

Recently, various wireless sensor networks have been developed for motor condition monitoring [8, 27, 28]. However the aim of most of these works is to detect the motor failure rather than the root of fault. The main challenge here is developing a computationally inexpensive system which can be implemented on industrial microprocessors.

In this research, a multi-sensor fusion framework is implemented on a wireless sensor node to detect multiple motor malefaction. This research emphasizes detailed diagnosis of the causes of the fault condition due to various bearing failure and air-gap eccentricity. The following sections review the state of the art in detection of each of these two faults.

2.1 Bearing Fault Detection

Bearing failures are the most common failures in induction motors [2]. The major causes of failures are: damages on inner or outer races of the bearing due to thermal or mechanical stresses. Misalignment and poor bearing fitting can also damage the bearing cage. The other source of bearing fault is lack of lubricant due to thermal or electrical stresses.

Various types of sensors and condition-monitoring methods have been developed for monitoring the bearing conditions. The most common method is to use vibration sensors to monitor the vibration of the bearings [24, 29–31].

Widodo et al. used a low speed bearing test rig to stimulate different bearing faults [24]. They used acoustic emission (AE) and vibration signals to train a support vector machine (SVM). Frosini and Bassi extended the bearing fault conditions to corrosion in bearing. They used stator current and efficiency of the induction motor for fault detection purposes [29].

Zhang et al. extracted entropy related features from vibration data [30]. They used a multi-scale entropy method, compared to regular entropy methods, provides information on nonlinear dynamics of the rotating components and coupling effects between these components. Onel and Benbouzid used Park and Concorida transform to detect bearing related failures [32].

Most of these bearing fault analyses are based on the single point defects on the bearing which occurs at a relatively severe stage of bearing failure. Based on its location, a single point defect can lead to a specific vibration frequency as shown in equations (2.1-2.3) [33]:

$$f_{vo} = \frac{n f_r \left(D - d cos\beta\right)}{2D} \tag{2.1}$$

$$f_{vi} = \frac{n f_r \left(D + d cos\beta\right)}{2D} \tag{2.2}$$

$$f_{vb} = \frac{D}{d}\left[1 - \left(\frac{d}{D} cos\beta\right)\right] \tag{2.3}$$

Another method of detecting bearing faults can be obtained by noting that bearing vibration typically leads to variations in the motor torque which is related

to the current drawn by the motor. Thus the current harmonic at the specific frequencies will be affected by bearing vibration. The current spectrum can also be used to detect bearing failures as equation (2.4):

$$f_{current} = f_s \pm k f_c \tag{2.4}$$

Current signal is already being measured in motors with the speed controller and therefore does not need extra sensors. At the same time, the current spectrum includes information from other motor malfunctions such as load oscillation, broken rotor bar and rotor eccentricity. These extraneous sources can be removed by different methods such as Wiener filter-based noise cancellation [34] and statistical approaches [35].

2.2 Air-gap Eccentricity

Air gap eccentricity is a condition in which there is an uneven air gap between the stator and the rotor. Air-gap eccentricity unbalances the magnetic pull and causes vibration, acoustic noise, bearing wear and rotor deflection. Consequently, eccentricity may lead to severe damage to the stator and rotor core. Thus, it is critical to detect the air gap eccentricity at an early stage to protect the motor system. Static eccentricity is either caused by the ovality of stator core or incorrect positioning of stator core and/ or bearing. In static eccentricity, the position of minimum air-gap is fixed [36].

High level of static eccentricity may lead to dynamic eccentricity where the center of the rotor is not at the center of rotation, and the position of the minimum

air-gap rotates with the rotor. Other causes of dynamic air-gap eccentricity are bent shaft, worn bearings or asymmetric thermal expansion of the rotor [37].

Air gap eccentricity induces stator current harmonics at specific high and low frequencies [36]. High frequency component of interests can be described by equation 2.5.

$$f_{HE} = \left[\frac{1-s}{p}\left(kR \pm n_d\right)\nu\right] f_s \tag{2.5}$$

Where $n_d = 0$ for static eccentricity and $n_d = 1$, 2 or 3 for dynamic cases [22]. Furthermore, if both static and dynamic eccentricities exist together ,the case in most air-gap related failures, there will be low-frequency components near the fundamental frequency which can be expressed by equation 2.6:

$$f_{LE} = f_s \pm k f_r \tag{2.6}$$

In case of mixed eccentricity low frequency component can also be detected in stator vibration signal (equation 2.7) [22].

$$f_{VE} = 2f_s \pm k f_r \tag{2.7}$$

Different features such as instantaneous reactive power [37] have been introduced to detect the air-gap related problems in motor current signature analysis (MCSA). However, the main drawback of MCSA is that the load oscillation can also lead to current harmonics at frequencies described by (5), which is one of the major challenges in the eccentricity detection.

To eliminate the load effects from eccentricity detection, different method such as signal injection-based method [38] and monitoring both current and voltage harmonic [39] have been proposed. Additionally, Antonino and Pons-Llinares

proposed the analysis of startup current to detect eccentricity [12]. However, these methods are limited as they cannot provide continuous protection.

The goal of this project is to determine the feasibility of a stand-alone multi-sensor wireless system for continuous real-time performance and condition monitoring of induction motors.

The system employs multiple sensors mounted on a common wireless platform with the capability of installation inside the motor on the stator end-coils or outside on the test bed.

The system follows a sensor fusion approach to detect single faults or combinations of faults in their incipient stages and provides early warning of impending problems. The wireless system provides a low-cost alternative to expensive condition monitoring technology available through dedicated current signature analysis or vibration monitoring equipment. The key performance objectives for the wireless system are :

- Detect faults in induction motors with a probability of 99.9% (i.e. probability of missing a fault is less than 0.1%).
- Produce false alarms no more than 5%.
- Have a high accuracy ($> 99\%$) of correctly identifying the nature and severity of the fault. The faults of interest are static and dynamic air-gap eccentricity and bearing damage (inner-outer race damage, damage on cage or lack of lubricant).

Chapter 3

Material and Methods

The faults of interest in this research are air-gap eccentricity and bearing failure. Experiments are conducted under fifteen different conditions which are grouped as three categories:

- Faulty bearings (with 4 levels: bearing with no grease, bearing with damages on inner-race, outer-race and cage)
- Air-gap eccentricity condition (4 levels of static air-gap eccentricity and 6 levels of dynamic air-gap eccentricity)
- Normal condition.

Faulty bearing conditions are studied by replacing one of the bearings in the motor housing by a damaged one shown in Figure 3.1.

The effects of air-gap eccentricity are studied by replacing one or both of the bearings in the motor housing by modified bushings shown in Figure 3.1B. In this figure, bearings with off-centered outer bushing cause static eccentricity. The

Figure 3.1: A) Damaged bearings B) Bearings replacements for eccentricity

offset causes an uneven air-gap length between the rotor and the stator as shown in Figure 3.2. Different values of offsets create different air-gap lengths.

Moreover, replacing the bearings can be done in two different ways: keeping the thicker part of both bushes in the same direction or in opposite directions. The rotors axes of rotation will be more translated and less tilted when the thicker parts of the bearings are in the same direction and vice versa for the opposite direction as shown in Figure 3.2.

Two levels of dynamic eccentricity are used: one corresponding to the original bearings and one created by mounting the front bearing on inner and outer bushings with offsets (Figure 3.1).

Ten conditions of air-gap eccentricity (both static and dynamic) are chosen from the various ways to combine the offset bearings in the motor assembly.

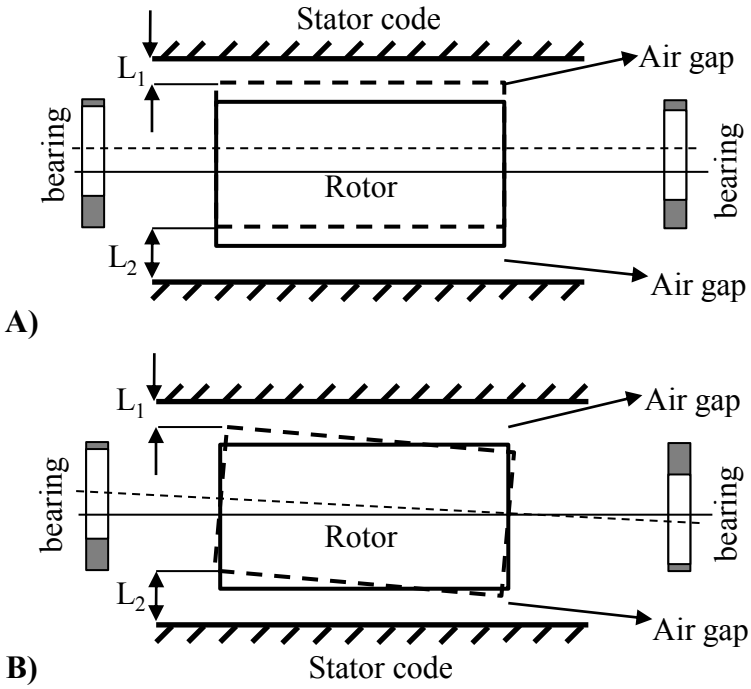

Figure 3.2: Static air-gap eccentricity where Axis of rotation is translated (A) or tilted (B).

The experiment is block randomized with 40 trials for the normal condition, 20 trials for each faulty bearing and 10 trials of each air-gap conditions. This means that one of the conditions is randomly selected and the experiments are conducted in 10 trials. Upon completing all the 10 trials, another condition is selected randomly again and the whole procedure is repeated. In each trial, the data are recorded in 2 minute time spans. The first and the last 10 seconds of the data are deleted to eliminate transitional effects. The remaining signal is then cut to 5 seconds segments. This process extracts 20 segments (data points) form each trial.

The recorded data can be summarized as follows:

- Normal condition (1-level) 40 trials (800 segments).

- Air-gap eccentricity (10-levels)100 trials (2000 segments).
- Faulty bearing (4-levels) 80 trials (1600 segments).

3.1 Experimental Setup

The motors used in the experiment are 1.5hp 6-pole 3-phase induction motor rated at 230V line voltage and 4.8A line current. They are connected to a PWM adjustable speed drive to control the speed. The running speed of the motors with no load is 1200 rpm (20 Hz). In addition to wireless sensor node, wired sensors (accelerometer, current and sound) are used to validate the data obtained from wireless sensors.

Finally, the experiment is conducted using two identical motors to remove effects related to the variability in the motors and also to validate the robustness of the classification algorithm. One of the motors is only used to record normal conditions while the other one is used to record both normal and faulty conditions. The experimental setup is shown in Figure 3.3.

To develop a wireless sensor network, Imote2 sensor nodes are used [40]. Imote2 is a modular platform and can be stacked with sensor boards to customize the system to a specific application, along with a power board to supply power to the system. The Imote2 consists of an Intel PXA271 XScale processor combined with 32MB of on-board Flash storage and 32MB of SRAM. The three layers (Imote2, sensor board and power board) of modular sensor node are shown in Figure 3.4A. The top and bottom view of the Imote2 board is also shown in Figure 3.4B.

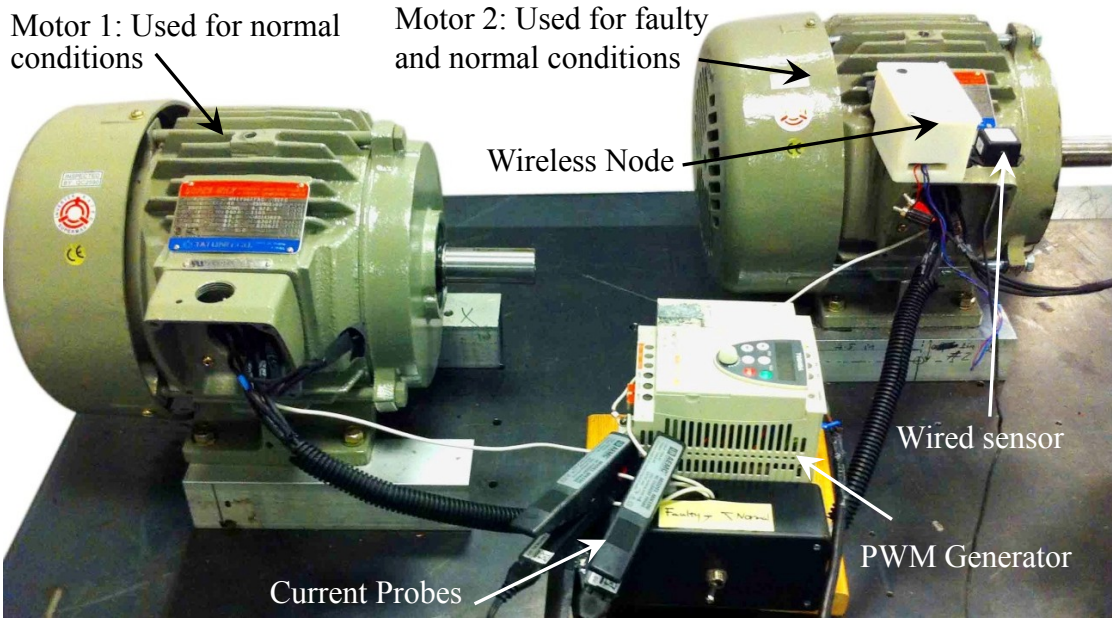

Figure 3.3: Experimental setup used in this study.

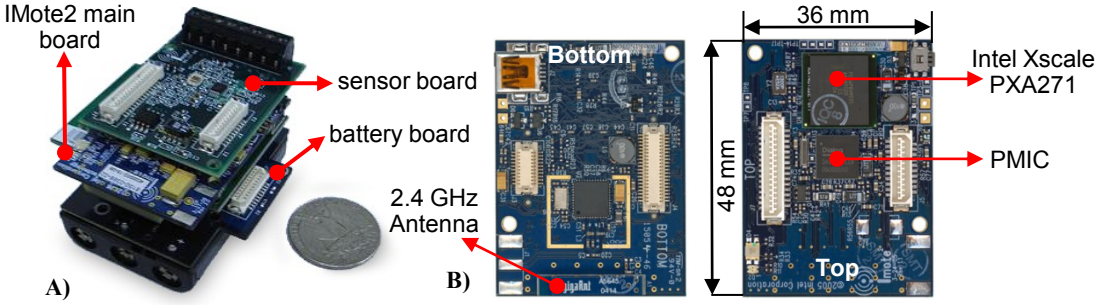

Figure 3.4: A) Three layer of modular sensor node B) Top and Bottom view of Imote2 main board.

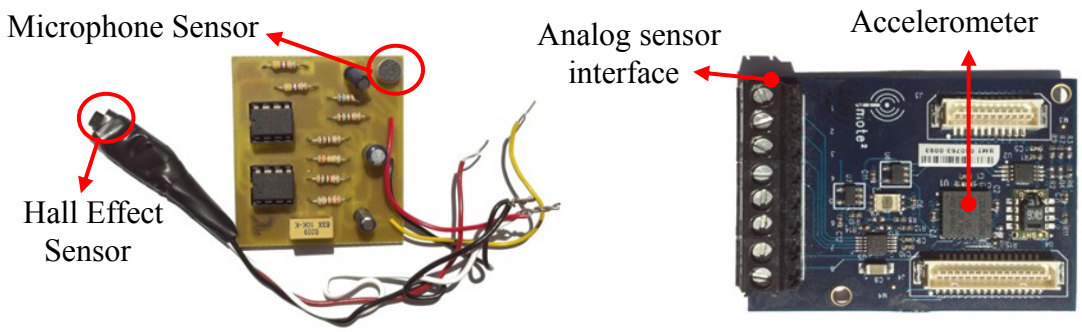

Figure 3.5: Crossbow sensor board and the external sensors connected to it.

The radio chip (CC2420) supports a 250 kb/s data rate with 16 channels in the 2.4 GHz band. The integrated antenna enables the sensor mote to provide a nominal range of about 30 meters. This sensor mote supports a variety of operation system options. The open source Tiny Operating System (TinyOS) is used for this study. This operating system executes programs independently written in the programming language nesC.

For data acquisition, Imote2 compatible sensor board manufactured by Crossbow Technology, Inc is used in this study (Figure 3.5). It contains a three-axis accelerometer and a 4 channel 12-bit Analog to Digital Converter (ADC) to which an external microphone and a hall-effect sensor are connected.

The acoustic signal is first passed through a high pass filter to remove DC components and is then amplified. To avoid aliasing, a low pass filter is used before the signal goes to the ADC. All the data are recorded at a sampling rate of 256 Hz.

The sensor continuously collects and buffers data for 4 seconds. When the buffer is full, the stored data is transmitted from the sensor node to the receiver

in the form of packets. When all the packets are sent out, the sensor node starts to collect data again. Each packet consists of the sensor node ID and the packet ID number, followed by the data processing. In the data area, 114 bytes is used for the collected data, one additional byte is used to mark the Cyclic Redundancy Check.

The signals from all three sensors are analyzed using two methods 1) The Hilbert Huang Transform (HHT) 2) Fast Fourier Transform (FFT). Unlike FFT, HHT provides information in joint time and frequency domains. The HHT has been shown to be especially useful for non-stationary signals [41].

3.2 Hilbert-Huang Transform

HHT adaptively tracks the evolution of the timefrequency in the original signal and provides detailed information at arbitrary timefrequency scales. HHT is computed in two steps: 1) Empirical mode decomposition (EMD) and 2) Hilbert spectral analysis.

HHT uses the EMD to decompose a signal into a finite set of intrinsic mode functions (IMFs), and then uses the Hilbert transform of the IMFs to obtain instantaneous frequency and amplitude data. Intrinsic Mode Functions (IMFs) are defined as a class of functions that satisfy two conditions:

- In the whole data set, the number of extrema and the number of zero crossings must be either equal or differ at most by one. (In other words, every adjacent local maxima and minima of the wave must across the zero line.)

- At any point, the mean value of the envelope defined by the local maxima and the envelope defined by the local minima is zero. (In other words, the upper envelope and the lower envelope estimated from the local maxima and local minima are approximately symmetric with regard to the zero line.)

To extract IMFs from the signal X(t), empirical mode decomposition uses a sifting process comprising the following steps:

- STEP1:

  a. Find the positions and amplitudes of local maxima, and local minima of $X(t)$.

  b. Construct an upper envelope by interpolation (typically a cubic spline interpolation) of the local maxima, and a lower envelope by a similar interpolation of the local minima.

  c. Calculate the mean $M_1(t)$ of the upper and lower envelopes.

  d. Subtracting the envelope mean signal from the original input signal, we have

$$h_1(t) = X(t) - M_1(t) \tag{3.1}$$

  e. Check whether $h_1(t)$ meets the requirements to be an IMF as defined in the section above. If not, treat $h_1(t)$ as new data and repeat the previous process. Then set

$$h_{11}(t) = h_1(t) - M_{11}(t) \tag{3.2}$$

f. Repeat this sifting procedure k times until $h_{1k}(t)$ is an IMF; this is designated as the first IMF.

$$u_1(t) = h_{1k}(t) \tag{3.3}$$

- STEP2

  a. Subtract $u_1(t)$ from the input signal and define the remainder, $r_1(t)$, as the first residue. Since the residue, $r_1(t)$, still contains information related to longer period components, it is taken as a new data stream. Repeat the described sifting process in step 1 to find more IMFs.

  b. The sifting process is stopped when either of the following criteria are met: 1) the component $u_n(t)$, or the residue $r_n(t)$, becomes so small in magnitude as to be considered inconsequential, or 2) the residue, $r_n(t)$, becomes a monotonic function from which an IMF cannot be extracted.

Using the EMD method, a time series signal $x(t)$ is represented as a sum of n IMFs $u_i(t)$ and a residue r as shown in Equation 3.4. The sifting process in empirical mode decomposition is shown in Figure 3.6

$$X(t) = \sum_{i=1}^{n} u_i(t) + r \tag{3.4}$$

Having obtained the IMFs, the Hilbert transform is applied to each IMF component. Instantaneous amplitude $\alpha_i(t)$, phase $\theta_i(t)$ and frequency $\omega_i(t)$ can be expressed as Equation 3.5–3.7.

$$\alpha_i(t) = \sqrt{u_i(t)^2 + H[u_i(t)]^2} \tag{3.5}$$

$$\theta_i(t) = tan^{-1}\frac{H[u_i(t)]}{u_i(t)} \tag{3.6}$$

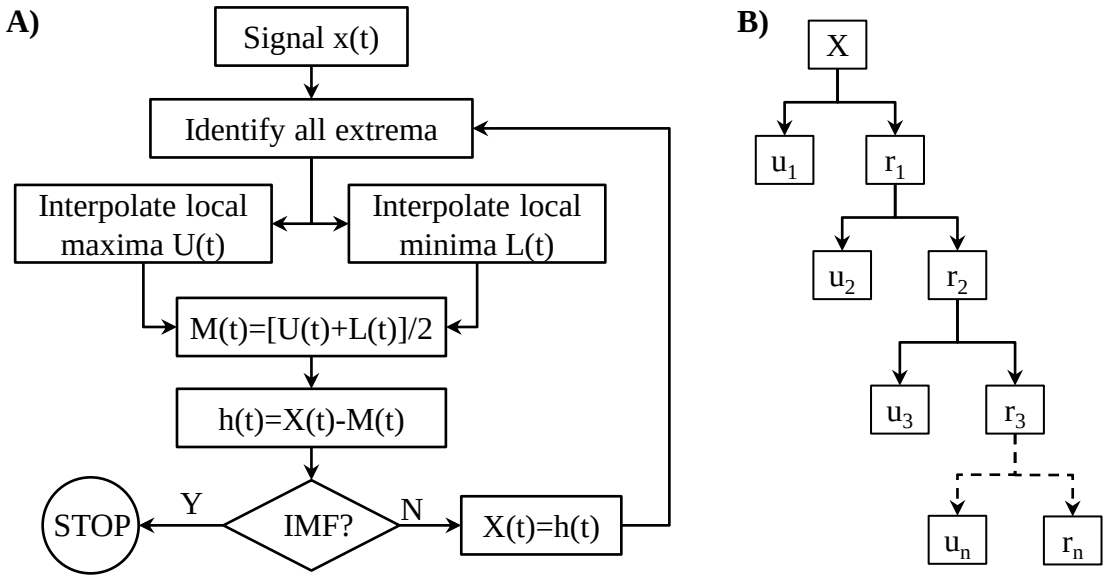

Figure 3.6: A) Siftting method for finding each IMF. B) Empirical Mode Decomposition of the signal to n IMF

$$\omega_i(t) = \frac{d\theta_i(t)}{dt} \tag{3.7}$$

Figure 3.7 illustrates the IMF extracted from vibration signal. As shown in Figure 3.7, the IMFs are sorted in descending order of frequency associated with the locally highest frequency and with the lowest frequency.

The frequency-time distribution of the amplitude over different IMFs is designated as the Hilbert Spectrum . Finally the marginal spectrum is computed as Equation 3.8.

$$h(\omega) = \int_0^T H(\omega, t)\,\mathrm{d}t. \tag{3.8}$$

Using the Hilbert marginal spectrum (HMS), a feature vector consist of the instantaneous power of nine different frequencies bands in the first two IMF along with the average amplitude of the first two IMF for each signal is calculated. The

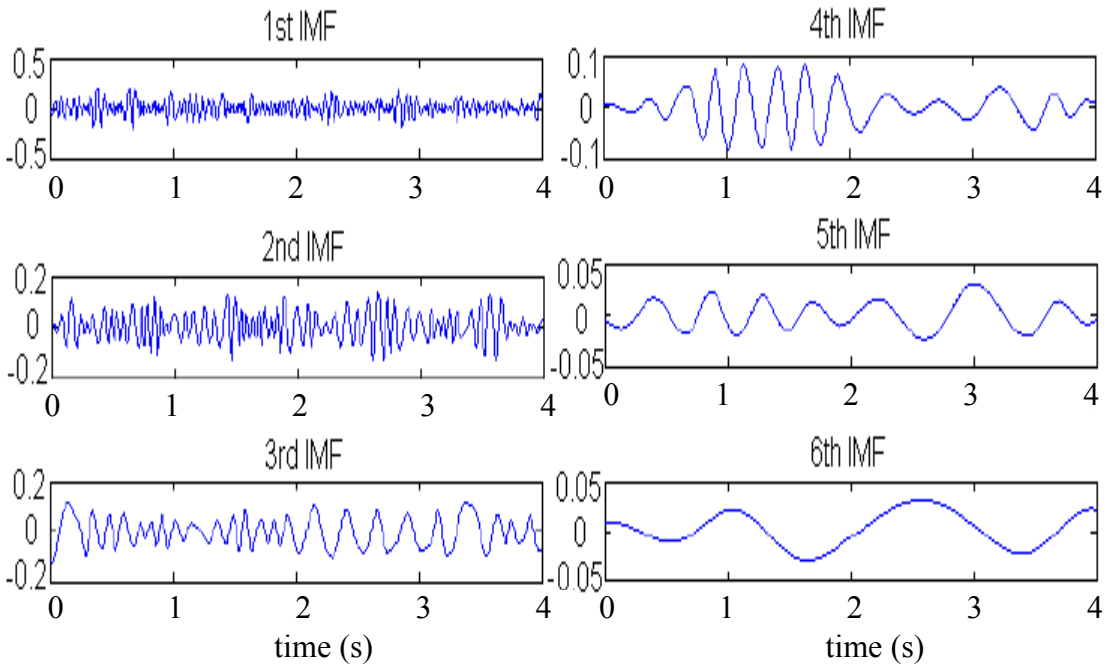

Figure 3.7: Different IMF of vibration signal in normal condition.

average instantaneous amplitude can be expressed as equation 3.9:

$$\bar{\alpha_i} = \frac{1}{N} \sum_{n=1}^{N} \alpha_i(n) \tag{3.9}$$

3.3 Feature Extraction

The relevant features that carry the fault information depend upon the combination of sensor and signal processing algorithms. To extract the fault information, the feature extraction method is based on fault characteristic frequencies of the motor (f_{vo},f_{vi},f_{vb}) and the low characteristic frequencies of air-gap eccentricity (f_{LE}). The high-frequency components related to air-gap eccentricity (in kHz) require sensors with high sampling rates and an undesirable increase the com-

putational complexity. Therefore low frequency components near the supplied frequency (f_s= 60 Hz) are used in the feature extraction method.

The bearing used in the experiment is SKF bearing of series 6206, a deep grove ball bearing containing 9 balls. The contact angle is 0^o. The ball diameter is 9.525mm and the pitch diameter is 46mm. Using equations 2.1-2.7, the inner/outer race fault characteristic frequencies in signal are determined as 108.63Hz and 71.36 Hz respectively. The ball spin frequency is 46.22 Hz in vibration and 13.78 Hz in current signals. Also the eccentricity related frequencies of interest are determined as 20, 40, 60, 80 and 100 Hz.

A frequency band centered at each of the nine frequencies of interest, with a width of 2 Hz is used to calculate the power spectral density from the FFT analysis. Power spectral density of each frequency band is then normalized with respect to the power of the whole signal to form the first feature sets.

Hilbert marginal spectrum of the first extracted IMF is also calculated using the same frequency bands. Due to lack of high frequency components in the second IMF, only the Hilbert marginal spectral at 20 and 40 Hz are calculated in the second IMF. Finally the averaged instantaneous amplitudes of the first two IMFs are selected as the last set of features. Table 3.1 lists all the features which are generated from each sensor based on the fault characteristic frequencies.

As Table 3.1 illustrates, there are 23 features extracted from each sensor. This forms a feature vector of size 92 for each segment of data.

In order to reduce the computational complexity as well as the number of free parameters in the classifier (e.g. classifiers weights), it is necessary to find the

Table 3.1: List of Features extracted from each sensor

Type	Feature Details
FFT	PSD at 13.78, 20, 40, 46.22, 60, 71.36, 80, 100 and 108.63 Hz
HHT	HMS at 13.78, 20, 40, 46.22, 60, 71.36, 80 ,100, 108.63 Hz of 1st IMF HMS at 13.78, 20 and 40Hz in the 2nd IMF Average instantaneous power of the 1st and 2nd IMF

best subset of features which has minimum mutual information and maximum class discriminatory information. To do so, a sequential forward search (SFS) is used for feature selection.

Starting from an empty feature set, SFS creates candidate feature subsets by sequentially adding each of the features not yet selected. For each candidate feature subset, 10fold cross-validation is performed by repeatedly checking the performance of a Fishers Linear Classifier (LDA) in separating the data of normal conditions from the faulty ones. Feature selection continues until there is no improvement in performance of LDA.

Using the SFS method, a subset of 8 features (out of 92 features) is determined as the best feature set. To further reduce the dimension of the features and to minimize mutual information, principal component analysis (PCA) is used to de-correlate the extracted features. Principal component identifies the main directions in the feature space where the data are distributed. Furthermore, similar feature extraction scheme is used to determine the subcategory of eccentricity and bearing fault. The feature selection scheme for faulty bearing condition is

based on the LDA performance in distinguishing between lubricant problem and any other bearings faults. Using the SFS method, PSD of vibration data at 71.36 Hz and average power envelope of first IMF of sound and vibration data are the best subset for bearing's fault.

In eccentricity-related fault; the goal of feature selection is to maximize the distance between dynamic and static eccentricities. SFD method selects the average power envelope of first IMF of vibration and PSD of vibration at 80Hz as the best features.

3.4 Classification

Based on the separability properties of the data, a two stage classification is used to detect the motor fault and its type. Figure 3.8 illustrates the complete classification process.

As shown in Figure 3.8, the recorded features are first classified by a linear classifier. The aim of this linear classifier is to project the data into a new hyper-axis such that the projected data have the maximum distance between classes and minimum distance within class. It uses a hyper-plane to separate the normal condition class from faulty conditions. This technique has a very low computational requirement which makes it suitable for fast fault detection and implementation on wireless nodes.

Additionally, if the data are classified as bearing fault or eccentricity, a kernel based support vector machine (SVM) is used as a secondary classification to detect

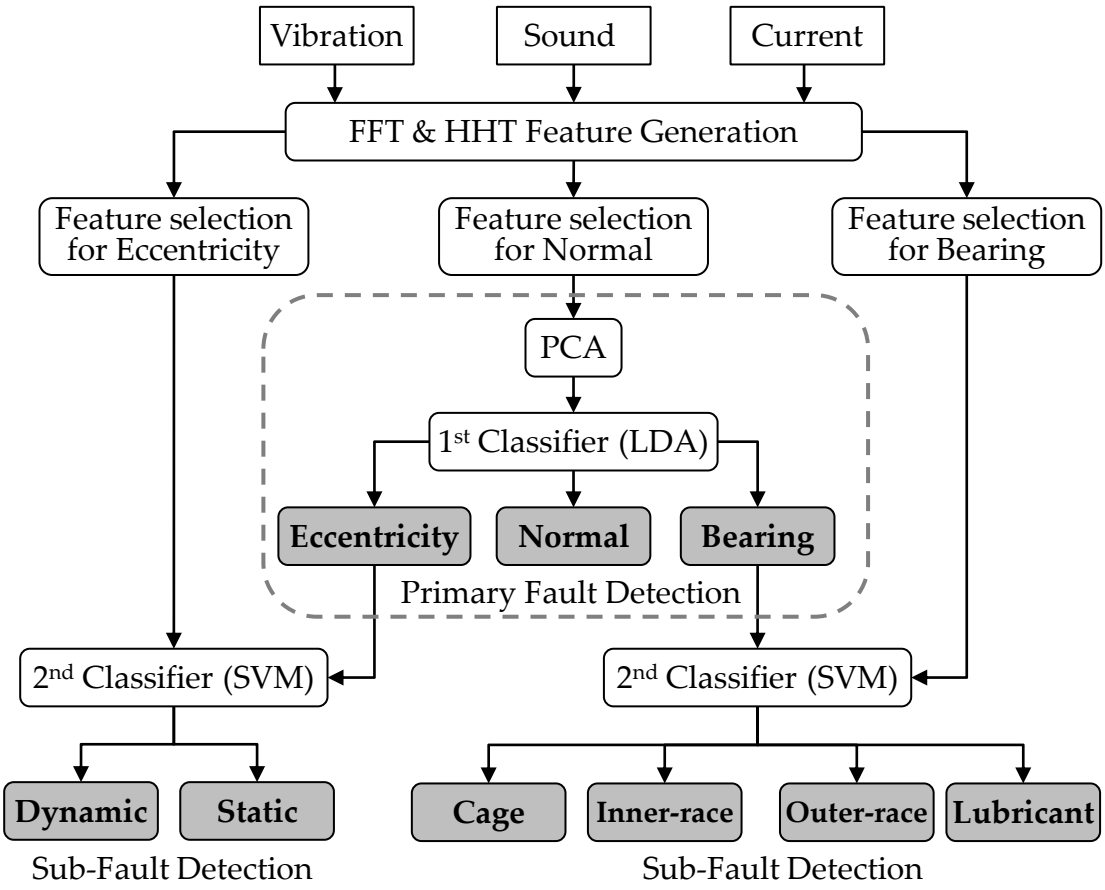

Figure 3.8: Classification Algorithm.

the fault sub-category. It should be noted that different feature vectors are used in primary and secondary classifiers.

Chapter 4

Results

Using the feature extraction/selection method, the first two principle components of FFT and HHT features can clearly separate the normal condition from air-gap and faulty bearings (inner/outer scratched, cage damaged and no lubricant conditions). Therefore, the first two PCA are used for the primary fault detection. Figure 4.1 illustrates the performance of the first two principle components in separating the data with different conditions.

Ten percent of all recorded data are used to train the classifiers and the remaining 90% to evaluate the performance of the classifier. A multi-class linear (LDA) and quadratic (QDA) discriminant analysis are used for the primary classification. The classification results are shown in Figure 4.2.

The white area in Figures 4.2 is the area classified as the normal condition. Also, the black and gray areas represent the feature subspace associated with eccentricity and bearing fault respectively. The boundary of the classes is represented by white dashed lines in LDA and solid contours in QDA.

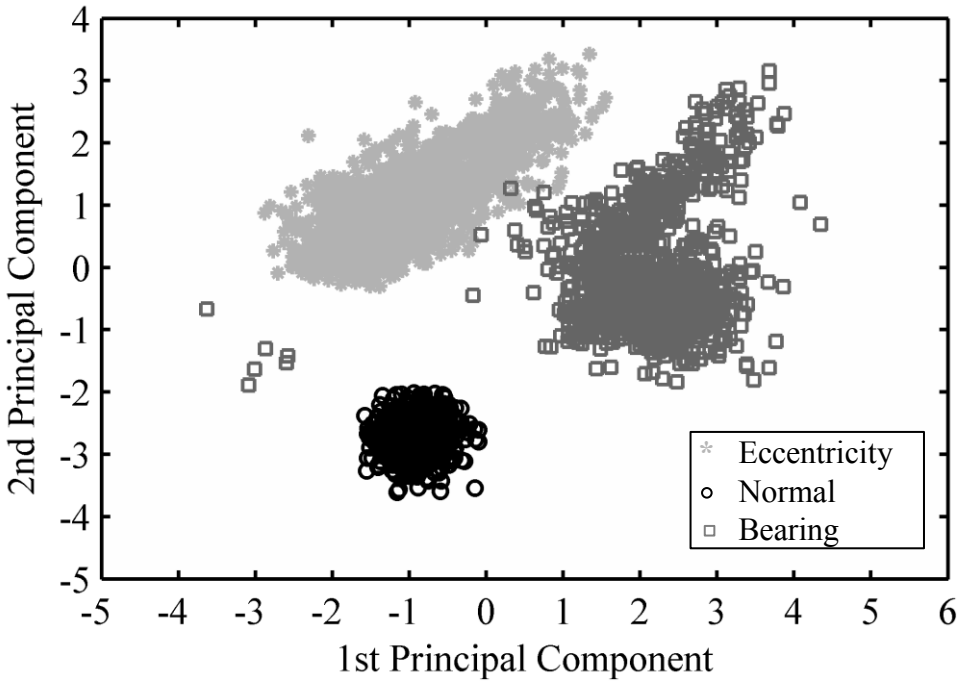

Figure 4.1: PCAs of features separating the normal condition from faulty conditions data.

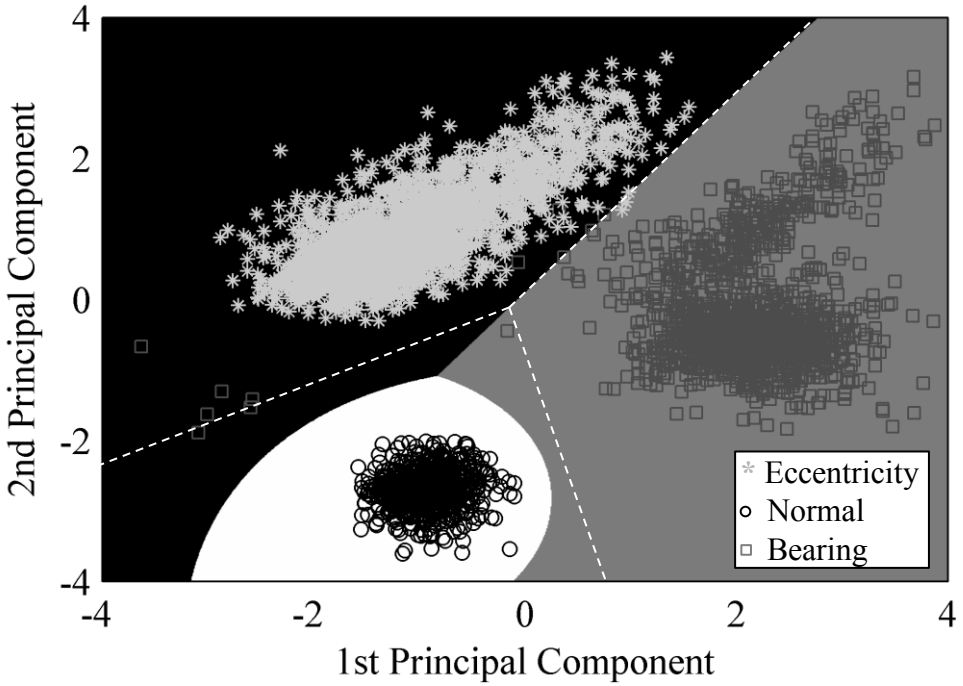

Figure 4.2: Multi-class LDA for primary fault detection (dashed line) and Multi-class QDA for primary fault detection (solid contour line)

It can be seen that LDA misclassified some of the outliers because there was a larger within-class variance in fault conditions than in normal condition. In fact, both bearing and eccentricity faults consist of several subclasses. Because of the differences in the nature of these subcategories, the within-class variance of fault condition is larger than normal condition. This makes the decision surface in LDA less sensitive to faulty conditions. Therefore, the rate of missing faulty conditions will increase. However; QDA solves this problem by using contour as the decision surface. The proposed approach can correctly detect almost all faulty conditions from normal conditions (>99% accuracy).

Table 4.1 summarizes the average classification rate of the primary classifier in 100 different cross evaluations. Numbers in the parenthesis are the standard deviation. Rows are the true class and columns are the classification results. It can be seen from Table 2 that almost all the normal conditions are correctly classified. The rate of false alarm in fault detection is less than 0.1%. By increasing the number of training data to 20%, the false alarm decays to zero. Also, it can be seen that most misclassification are in bearing faults (around 1%) which are misclassified as eccentricity.

Table 2 summarizes the average classification rate of the primary classifier in 100 different cross evaluations. Numbers in the parenthesis are the standard deviation. Rows are the true class and columns are the classification results. It can be seen from Table 2 that almost all the normal conditions are correctly classified. The rate of false alarm in fault detection is less than 0.1%. By increasing the number of training data to 20%, the false alarm decays to zero. Also, it can

Table 4.1: Confusion matrix for primary classification (faulty Detection)

	Normal	**Bearing Problem**	**Eccentricity**
Normal	99.96 (0.11)	0.04 (0.11)	NA
Bearing Problem	NA	99.34 (0.26)	0.66 (0.26)
Eccentricity	NA	0.18 (0.19)	99.82 (0.19)

be seen that most misclassification are in bearing faults (around 1%) which are misclassified as eccentricity.

In the primary classification, SFS identified eight features as the best subset of features for fault detections. Among them, the following components have the highest weight in the first two principal components: HMS of the vibration signal (at 46 and 71 Hz of the first IMF) and certain key frequencies of the PSD of the current and sound data (40 and 20 Hs for sound, 60 Hz for current).

Upon the detection of the fault type, the second classifier determines the sub-category of the detected fault. Again 10% of the faulty conditions data are used for training and remaining are used for testing in a 10-fold cross validation. The average classification rate over 100 evaluations is presented in Table 4.2 for bearing fault and in Table 4.3 for eccentricity. The numbers in the parenthesis are the standard deviation. Rows are the real class and columns are the classification result.

It can be seen in Table 4.2, that almost all the lubricant problems have been classified correctly. This is not surprising as the feature set selected for this clas-

Table 4.2: Confusion matrix for secondary classification (Bearing Fault Type)

	Inner-race	**Cage**	**Outer-race**	**Lubricant**
Inner-race	95.7 (2.5)	3.9 (2.5)	0.4 (0.6)	NA
Cage(Side)	37.0 (4.8)	60.2 (5.2)	2.8 (2.1)	NA
Outer-race	NA	11.6 (2.7)	88.4 (2.7)	NA
Lubricant	NA	0.1 (0.1)	NA	99.9 (0.1)

sifier is based on the separability of this kind of fault (lack of lubricant) from the other types.

Figure 4.3 shows that inner-race and outer-race scratched cases are almost in two separate clusters. This explains their high accuracy rate (95.7% and 88.4% respectively). Furthermore, the damage on the bearing's cage has the lowest classification rate. It is mostly confused with inner-race damage. This is mostly because of the distribution of this fault (Figure 4.3) which forms two main clusters. The larger cluster is well separated from the other faults while the second one (which is smaller in size and larger in variance) is projected on the outer-race condition. It can also be interpreted from Table 4.2, that cage damage, is the only condition with which all other bearing fault are confused, probably because the procedure for changing the bearings in different experimental setups can damage the cage.

Finally the confusion matrix for the last category of motor malfunction, eccentricity, is illustrated in Table 4.3.

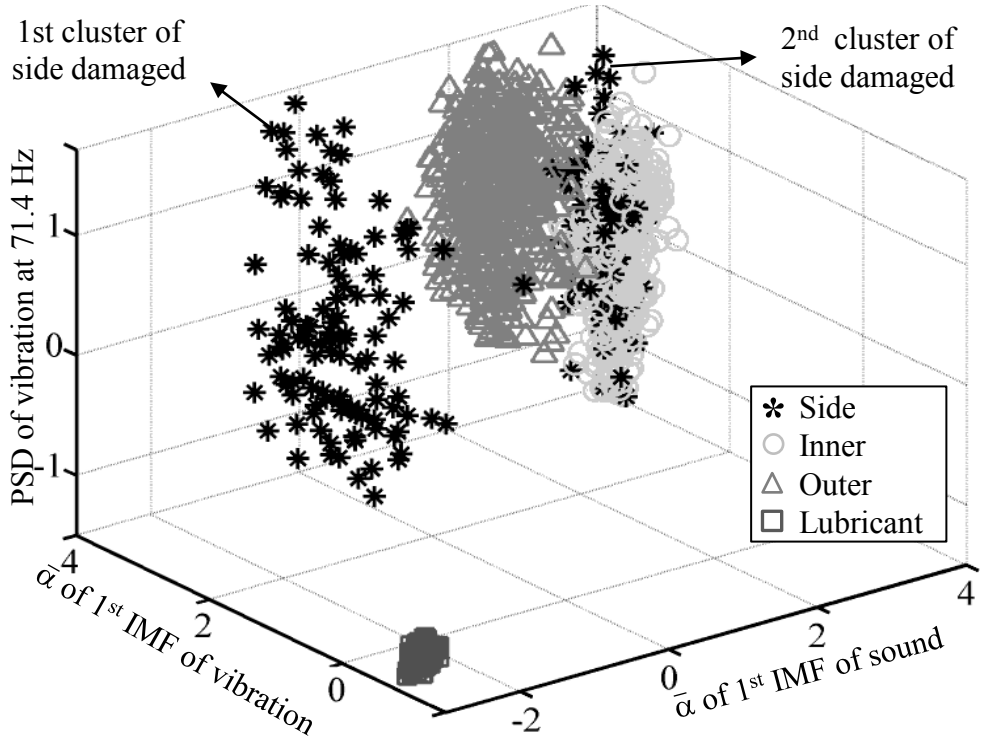

Figure 4.3: Features separating subclasses of bearing damages.

Table 4.3: Confusion matrix for secondary classification (Eccentricity Fault Type)

	Static Eccentricity	**Dynamic Eccentricity**
Static Eccentricity	97.4 (0.6)	2.6 (0.6)
Dynamic Eccentricity	11.9 (2.3)	88.1 (5.2)

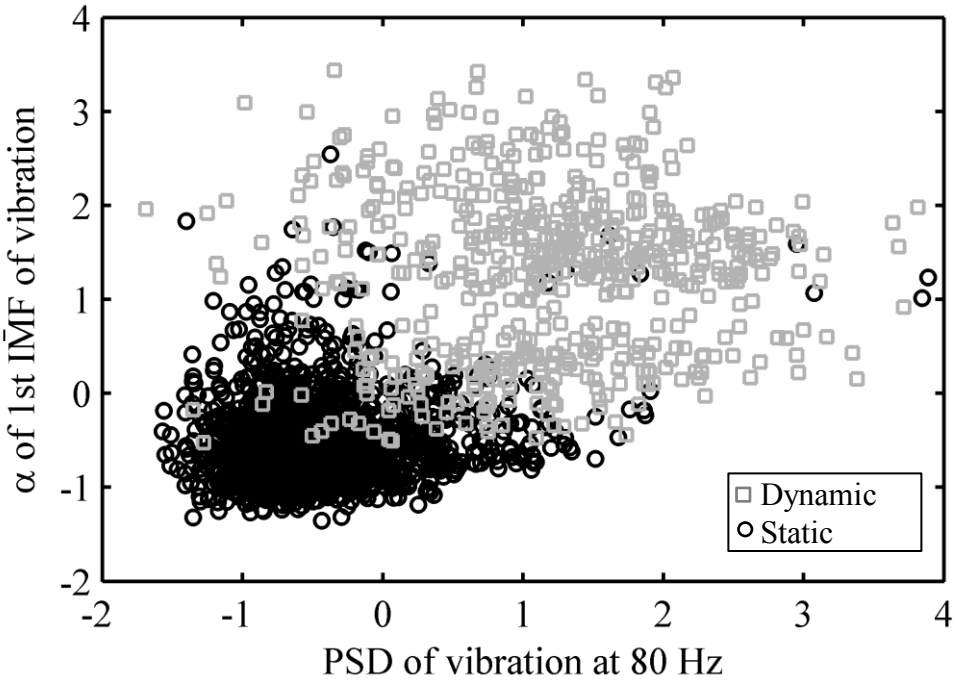

Figure 4.4: SVM classifier for distinguishing between static and Dynamic Eccentricity.

Table 4.3 shows that the SVM classifier can achieve high accuracy in static and dynamic eccentricity (97% and 89% respectively). Moreover, Figure 4.3 illustrates the classification of feature space with only considering two vibration based features: PSD at 80HZ and average power of the first IMF.

Figure 4.4 illustrate the distribution of the dynamic and static eccentricity in the related feature space. It can be seen that static and dynamic eccentricities have distinguishable mean value but large standard deviation which eventually cause confusion in the classification. This is possibly because of excluding the high frequency components from the feature space for reduceing the computational demand.

Chapter 5

Conclusions

The proposed research develops an inexpensive multi-sensor wireless sensor system to perform real-time condition monitoring of induction motors. The use of multiple sensor modalities reduces the need for precise instrumentation and signal processing as information from several sources are extracted.

The results showed that a combination of the intrinsic mode functions of the HHT of the vibration signal and certain key frequencies of the FFT of the current and sound data yield the highest accuracy. The proposed wireless system can distinguish a faulty motor from a healthy motor with a probability of 99.9% with less than 0.1% likelihood of false alarm. It can also discriminate between different fault categories and severity with in a high accuracy. Bearing and eccentricity fault can be detected with 99.9% accuracy. Within bearing fault, the lack of lubricant in bearing and damage on Inner and outer-race of the bearing can be detected with an average accuracy of 95%. The accuracy of faulty bearing with side damage is relatively low (60%).

However, as long as bearing fault is not misclassified as normal or eccentricity, the confusion between bearing with Inner/outer and side damage is not, practically speaking, an issue because, in any case of bearing damage, the bearing needs to be replaced.

5.1 Future Direction

There are some motor malfunctions which are not considered in this study. Future research should considered Rotor bar damage and Stator winding imbalance, in the fault detection algorithm.

The current experiments in this research only considered constant loading and constant speed. Although in most of the industrial applications this can be a good assumption, future works should take the variable speed and loading into account. This consideration will make the condition monitoring system more robust to possible uncertainties in the system.

In this research a single sensor node is used to provide high-level status and diagnostic information for maintenance personnel. In future research, these individual wireless sensors can be incorporated into a sensor network involving nodes from other parts of the machine or from other machines to coordinate condition monitoring.

A basic issue that is identified by our previous feasibility studies on wireless sensors [42] was their limited battery life when they were required to transmit raw data signals to the base station. This limitation is partially solved by performing

all computations on the sensor node and thus eliminating the need to send raw signals. Future development will also include power management in the wireless sensor through sleep scheduling and energy scavenging from the fringing magnetic fields from the stator end-coils [43].

Bibliography

[1] R. Kothamasu and S. Huang, "Adaptive mamdani fuzzy model for condition-based maintenance," *Fuzzy Sets and Systems*, vol. 158, no. 24, pp. 2715–2733, 2007.

[2] P. Tavner, L. Ran, J. Penman, and H. Sedding, *Condition Monitoring of Rotating Electrical Machines,* 2nd. Stevenage, U.K.: IET, 2008.

[3] B. Lu, T. Habetler, and R. Harley, "A survey of efficiency-estimation methods for in-service induction motors," *IEEE Transactions on Industry Applications*, vol. 42, no. 4, pp. 924–933, 2006.

[4] B. Rao, *Handbook of condition monitoring.* Elsevier Science, 1996.

[5] "United States Industrial Electric Motor Systems Market Opportunities Assessment," *US DOE, Washington DC*, 1998.

[6] "California Energy Commission Database," *California Energy Commission*, 2009.

[7] M. Benbouzid and G. Kliman, "What stator current processing based technique to use for induction motor rotor faults diagnosis?," *IEEE Transactions on Energy Conversion*, vol. 18, no. 2, pp. 238–244, 2003.

[8] W. Wang and O. Jianu, "A Smart Sensing Unit for Vibration Measurement and Monitoring," *IEEE/ASME Transactions on Mechatronics*, vol. 15, no. 1, pp. 70–78, 2010.

[9] S. Al-Dossary, R. Hamzah, and D. Mba, "Observations of changes in acoustic emission waveform for varying seeded defect sizes in a rolling element bearing," *Applied acoustics*, vol. 70, no. 1, pp. 58–81, 2009.

[10] A. Garcia-Perez, R. Romero-Troncoso, E. Cabal-Yepez, R. Osornio-Rios, and J. Lucio-Martinez, "Application of high-resolution spectral-analysis for identifying faults in induction motors by means of sound," *Journal of Vibration and Control*, Oct. 2012, ISSN: 1077-5463.

[11] A. Garcia-Perez, R. de Jesus Romero-Troncoso, E. Cabal-Yepez, and R. Osornio-Rios, "The application of high-resolution spectral analysis for identifying multiple combined faults in induction motors," *IEEE Transactions on Industrial Electronics*, vol. 58, no. 5, pp. 2002–2010, 2011.

[12] J. Pons-Llinares, J. Antonino-Daviu, M. Riera-Guasp, M. Pineda- Sanchez, and V. Climente-Alarcon, "Induction motor diagnosis based on a transient current analytic wavelet transform via frequency b-splines," *IEEE Transactions on Industrial Electronics*, vol. 58, no. 5, pp. 1530–1544, 2011.

[13] Y. Wang, Z. He, and Y. Zi, "Enhancement of signal denoising and multiple fault signatures detecting in rotating machinery using dual-tree complex wavelet transform," *Mechanical Systems and Signal Processing*, vol. 24, no. 1, pp. 119–137, Jan. 2010.

[14] D. Ece and M. Basaran, "Condition monitoring of speed controlled induction motors using wavelet packets and discriminant analysis," *Expert Systems with Applications*, vol. 38, no. 7, pp. 8079–8086, Jul. 2011.

[15] S. Kia, H. Henao, and G. Capolinom, "Diagnosis of broken-bar fault in induction machines using discrete wavelet transform without slip estimation," *IEEE Transactions on Industry Applications*, vol. 45, no. 4, pp. 1395–1404, 2009.

[16] J. Antonino-Daviu, M. Riera-Guasp, M. Pineda-Sanchez, and R. Prez, "A critical comparison between DWT and Hilbert-Huang-based methods for the diagnosis of rotor bar failures in induction machines," *IEEE Transactions on Industry Applications*, vol. 45, no. 5, pp. 1794–1803, 2009.

[17] R. Yan and R. Gao, "Hilbert Huang Transform-Based Vibration Signal Analysis for Machine Health Monitoring," *IEEE Transactions on Instrumentation and Measurement*, vol. 55, no. 6, pp. 2320–2329, 2006.

[18] Y. Lei and M. Zuo, "Fault diagnosis of rotating machinery using an improved HHT based on EEMD and sensitive IMFs," *Measurement Science & Technology*, vol. 20, no. 12, p. 125 701, 2009.

[19] X. Zhao, T. Patel, and M. Zuo, "Multivariate EMD and full spectrum based condition monitoring for rotating machinery," *Mechanical Systems and Signal Processing*, vol. 26, no. 2, pp. 712–728, Feb. 2012.

[20] Z. Wang, J. Chen, G Dong, and Y. Zhou, "Constrained independent component analysis and its application to machine fault diagnosis," *Mechanical Systems and Signal Processing*, vol. 25, no. 7, pp. 2501–2512, Oct. 2011.

[21] A. Widodo, B. Yang, and T. Han, "Combination of independent component analysis and support vector machines for intelligent faults diagnosis of induction motors," *Expert Systems with Applications*, vol. 32, no. 2, pp. 299–312, Feb. 2007.

[22] S. Nandi, H. Toliyat, and X. Li, "Condition Monitoring and Fault Diagnosis of Electrical MotorsA Review," *IEEE Transactions on Energy Conversion*, vol. 20, no. 4, pp. 719–729, 2005.

[23] P. Zhang, Y. Du, T. Habetler, and B. Lu, "A Survey of Condition Monitoring and Protection Methods for Medium-Voltage Induction Motors," *IEEE Transactions on Industry Applications*, vol. 47, no. 1, pp. 34–46, 2011.

[24] A. Widodo, E. Kim, J. Son, B. Yang, A. Tan, D. Gu, B. Choi, and J. Mathew, "Fault diagnosis of low speed bearing based on relevance vector machine and support vector machine," *Expert Systems with Applications*, vol. 36, no. 3, pp. 7252–7261, Apr. 2009.

[25] V. Ghate and S. Dudul, "Cascade Neural-Network-Based Fault Classifier for Three-Phase Induction Motor," *IEEE Transactions on Industrial Electronics*, vol. 58, no. 5, pp. 1555–1563, 2011.

[26] H. Razik, M. Beltrao, and E. Roberto, "A novel monitoring of load level and broken bar fault severity applied to squirrel-cage induction motors using a

genetic algorithm," *IEEE Transactions on Industrial Electronics*, vol. 56, no. 11, pp. 4615–4626, 2009.

[27] B. Lu and V. Gungor, "Fault Diagnostics Using Wireless Sensor Networks," *IEEE Transactions on Industrial Electronics*, vol. 56, no. 11, pp. 4651–4659, 2009.

[28] V. Gungor, B. Lu, and G. Hancke, "Opportunities and Challenges of Wireless Sensor Networks in Smart Grid," *IEEE Transactions on Industrial Electronics*, vol. 57, no. 10, pp. 3557–3564, 2010.

[29] L. Frosini and E. Bassi, "Stator Current and Motor Efficiency as Indicators for Different Types of Bearing Faults in Induction Motors," *IEEE Transactions on Industrial Electronics*, vol. 57, no. 1, pp. 244–251, 2010.

[30] L. Zhang, G. Xiong, H. Liu, H. Zou, and W. Guo, "Bearing fault diagnosis using multi-scale entropy and adaptive neuro-fuzzy inference," *Expert Systems with Applications*, vol. 37, no. 8, pp. 6077–6085, Aug. 2010.

[31] B. Zhang, C. Sconyers, C. Byington, R. Patrick, M. Orchard, and G. Vachtsevanos, "A Probabilistic Fault Detection Approach : Application to Bearing Fault Detection," *IEEE Transactions on Industrial Electronics*, vol. 58, no. 5, pp. 2011–2018, 2011.

[32] I. Onel and M. El Hachemi Benbouzid, "Induction motor bearing failure detection and diagnosis: park and concordia transform approaches comparative study," *IEEE/ASME Transactions on Mechatronics*, vol. 13, no. 2, pp. 257–262, 2008.

[33] T. Harris, *Rolling Bearing Analysis*, 4th. Wiley, 2001, p. 1086.

[34] W. Zhou, T. Habetler, and R. Harley, "Bearing fault detection via stator current noise cancellation and statistical control," *IEEE Transactions on Industrial Electronics*, vol. 55, no. 12, pp. 4260–4269, 2008.

[35] F. Immovilli, M. Cocconcelli, A. Bellini, and R. Rubini, "Detection of generalized-roughness bearing fault by spectral-kurtosis energy of vibration or current signals," *IEEE Transactions on Industrial Electronics*, vol. 56, no. 11, pp. 4710–4717, 2009.

[36] D. Dorrell, W. Thomson, and S. Roach, "Analysis of airgap flux, current, and vibration signals as a function of the combination of static and dynamic airgap eccentricity in 3-phase induction motors," *IEEE Transactions on Industry Applications*, vol. 33, no. 1, pp. 24–34, 1997.

[37] M. Drif and A. Cardoso, "The use of the instantaneous-reactive-power signature analysis for rotor-cage-fault diagnostics in three-phase induction motors," *IEEE Transactions on Industrial Electronics*, vol. 56, no. 11, pp. 4606–4614, 2009.

[38] D. Hyun, J. Hong, S. Lee, K. Kim, E. Wiedenbrug, M. Teska, and S. Nandi, "Automated Monitoring of Airgap Eccentricity for Inverter-Fed Induction Motors Under Standstill Conditions," *IEEE Transactions on Industrial Electronics*, vol. 47, no. 3, pp. 1257–1266, 2011.

[39] X. Huang, T. Habetler, and R. Harley, "Detection of rotor eccentricity faults in a closed-loop drive-connected induction motor using an artificial neural

network," *IEEE Transactions on Power Electronics*, vol. 22, no. 4, pp. 1552–1559, 2007.

[40] *Intel Mote2 Overview, Version 3.0*. Intel Corporation Research, Santa Clara, CA, 2005.

[41] N. Huang and N. Attoh-Okine, *The Hilbert-Huang transform in engineering*. CRC Press, 2005.

[42] X. Xue, V. Sundararajan, and W. Brithinee, "The application of wireless sensor networks for condition monitoring in three-phase induction motors," in *Electrical Insulation Conference and Electrical Manufacturing Expo, 2007*, IEEE, 2007, pp. 445–448.

[43] A. Wickenheiser, T. Reissman, W. Wu, and E. Garcia, "Modeling the effects of electromechanical coupling on energy storage through piezoelectric energy harvesting," *IEEE/ASME Transactions on Mechatronics*, vol. 15, no. 3, pp. 400–411, 2010.